CERN-ACC-NOTE-2019-0024

2019.06.17

marco.d'andrea@cern.ch

Crystal Collimation Tests with Pb Ion Beams

M. D'Andrea, D. Mirarchi, S. Redaelli, A. Fomin, E. Belli, B. Salvachua Ferrando, L. Nevay, R. Rossi, W. Scandale, S. Montesano, F. Galluccio, P. Serrano Galvez, C. Dionisio Barreto, M. Butcher, I. Lamas Garcia
CERN, Geneva, Switzerland

Keywords: LHC, collimation, crystal, UA9

Summary

During MD4168, performed on November 27$^{\text{th}}$ 2018, silicon crystals for a crystal-assisted collimation system were tested. Crystal collimation is studied as an alternative scheme for ion collimation at the HL-LHC. Tests with ion beams at the LHC are fundamental to assess the performance of the system in view of a possible inclusion in future upgrades.

1 Introduction

The crystal collimation concept relies on the usage of bent crystals that can deflect halo particles at large angles of up to tens of μrad, as opposed to the standard LHC multi-stage collimation where an amorphous primary collimator scatters halo particles at a few μrad onto several secondary collimators. Crystal primaries could in principle send halo particles coherently onto a single absorber. A setup that uses only existing secondary collimators as absorbers for the channeled beam has been conceived for crystal collimation beam tests in IR7 [1]. Between 2015 and 2018, four bent crystals were installed in IR7, one for each cleaning plane on both Beam 1 and Beam 2. During the years, these crystals were tested and channeling was successfully observed at injection and top energy for both proton and ion beams. The main goal of this MD was to assess the performance of crystal-assisted collimation with ions at the LHC. After a first set of measurements aimed to fully characterize the crystal devices with Pb beams, an extensive campaign of loss maps was carried out in order to compare the standard and crystal-assisted system with different collimator settings. Crystals were also left in the beam line during the squeeze and with sustained losses on all four planes at the same time. Tests with high intensity beam were originally planned for this MD. However, they were dropped in favor of more measurements during the last fill at flat top energy, especially since similar tests were already previously carried out during the

intensity ramp up.

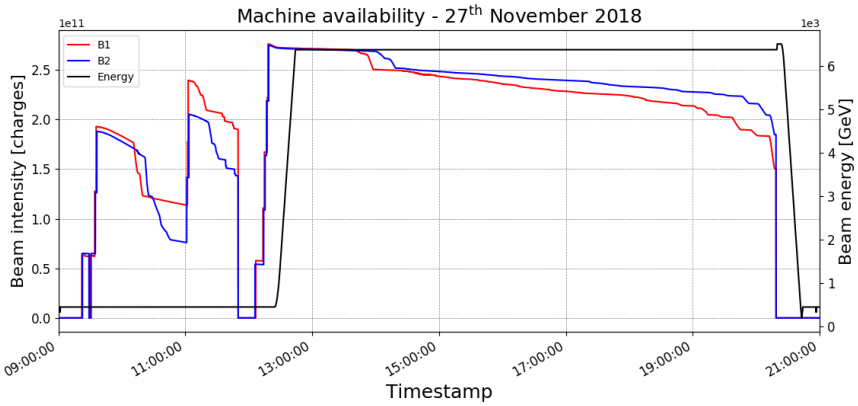

Figure 1: Beam 1 and Beam 2 intensity and energy during the MD.

2 Beam Setup

The MD was performed using several low-intensity bunches at both injection and flat top energy with standard 2018 optics for both Beam 1 and Beam 2, in a configuration that was extensively tested in previous crystal MDs [2–6]. The transverse dumper (ADT) was used to excite the beam with white noise, as in standard collimation loss maps, to achieve controlled primary beam losses on crystals and/or collimators. To have enough losses for the time needed to complete measurements such as angular scans, the ADT window was enlarged to act on three different bunches. This allows to achieve sufficiently high loss rates for longer times. For this reason, the filling scheme consisted of trains of nominal bunches with 2 μs spacing between bunches and 3 μs spacing between trains. For machine protection reasons, up to 30 bunches with total intensity below $3 \cdot 10^{11}$ charges are allowed at flat top. At injection nominal bunches can be used respecting the limit of $5 \cdot 10^{11}$ charges.

The scheduled measurements involved the following main activities:

1. beam-based alignment of the crystal with respect to the beam orbit and transverse positioning as primary collimator;
2. angular scan to find the optimal channeling condition;
3. transverse scan of the channeled beam with a secondary collimator;
4. cleaning measurements through loss maps with the crystal in channeling position and different collimator settings;
5. squeeze with crystals in channeling orientation;
6. sustained losses on all four planes at the same time with crystals in channeling orientation.

Fig. 1 shows the intensity and energy of the beams during the MD, which was excellent and allowed to carry out the full program. High intensity tests originally foreseen were dropped in favour of more measurements with the last fill at flat top energy.

3 Angular scans

Angular scans were performed for all crystals both at injection and at flat top. The optimal channeling orientation and reduction factor were measured for all four of them and are reported in Tab. 1. Fig. 2 and 3 show the angular scans of all crystals at injection and flat top respectively. The channeling orientation was efficiently found in agreement with previous measurements [7,8] except for the vertical crystal on Beam 2. This devices required a reboot of the goniometer some time before the MD, losing previously measured references. For this reason, the optimal channeling orientation for this crystal needed to be found from scratch both at injection and at flat top energy.

	Reduction factor		**Optimal channeling orientation [μrad]**		**Bending angle [μrad]**		**Multiturn CH efficiency**	
	Inj	**FT**	**Inj**	**FT**	**Inj**	**FT**	**Inj**	**FT**
B1H	7.4	4.5	1657.6	1618.7	64.7	64.5	~88%	~17%
B1V	4.6	3.4	2584.6	2532.1	45.7	40.9	~90%	~82%
B2H	3.7	2.6	-3386.4	-3474.9	41.8	36.4	~93%	~91%
B2V	14.8	3.5	351.2	314.3	54.3	53.1	~89%	~85%

Table 1: Reduction factor, optimal channeling orientation and bending angle calculated from measurements for all four crystals, both at injection and at flat top energy.

4 Linear Scans

Linear scans were performed with all four crystals both at injection and flat top energy. Fig. 5 and 4 show the scans and the measured bending angle are reported in Tab. 1. The results are consistent with previous measurements [7,8].

A significant difference can be observed in the measured channeling efficiency for the horizontal crystal on Beam 1 at injection and flat top energy. This is due to this crystal having a larger bending angle than the required specifics of 50 μrad because of an instability of the holder. In this situation, the bending radius is smaller than originally planned and at flat top energy it is too close to the critical radius. For this reason, the dechanneling probability is enhanced at flat top energy, while no significant effect is observed at injection. The dechanneling population can be seen in Fig. 5 as a rise in the BLM signal as the absorber moves closer to the primary beam. This is not the case for the other three devices, since their bending angle is closer to specifics or smaller.

The bending angle of the horizontal crystal in Beam 2 is found to be below the required specifics at injection and even smaller at flat top energy. This behaviour was already observed in earlier MDs [7,8] and it is not yet completely understood. It could be linked to the high miscut angle of this crystal, but this needs to be reproduced in simulations to provide a

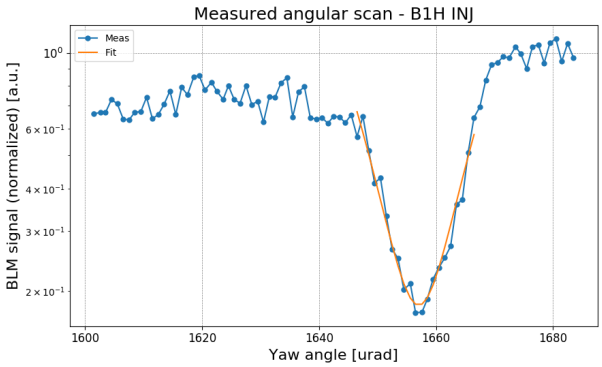

(a) B1H

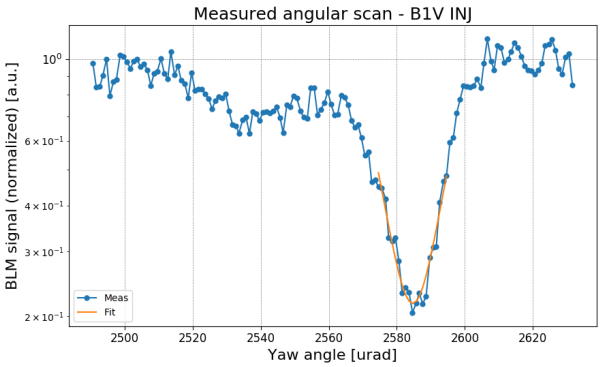

(b) B1V

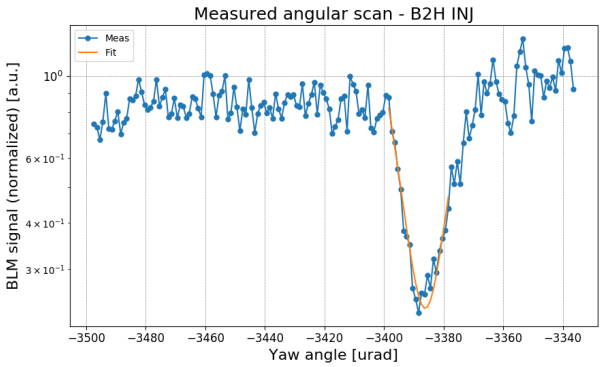

(c) B2H

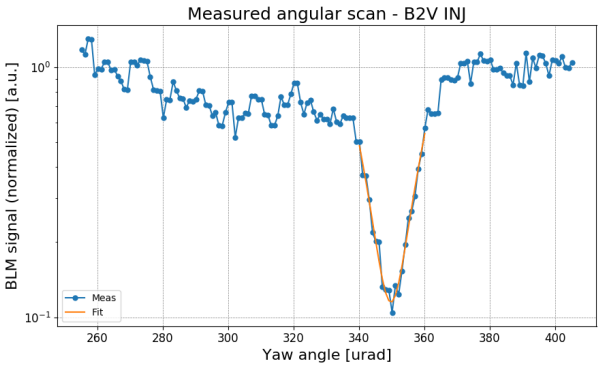

(d) B2V

Figure 2: Angular scans at injection energy. The BLM signal has been normalized to the particle flux and to the amorphous level.

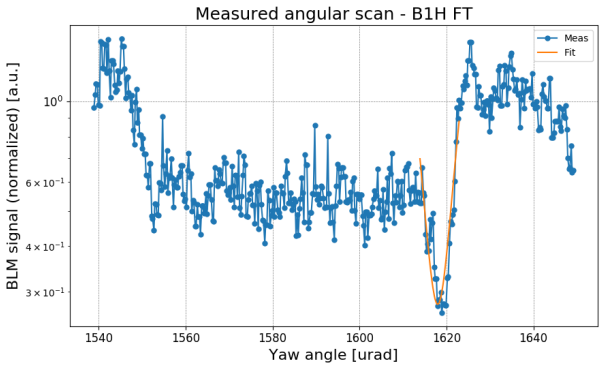

(a) B1H

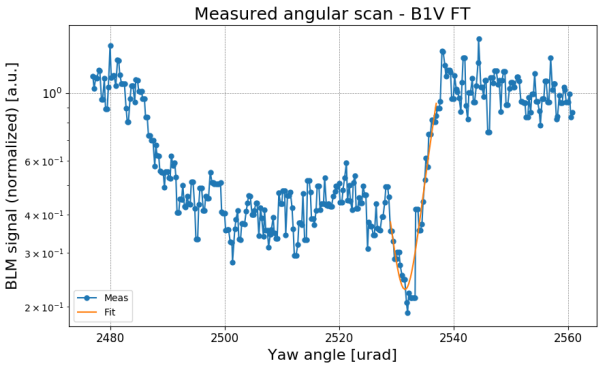

(b) B1V

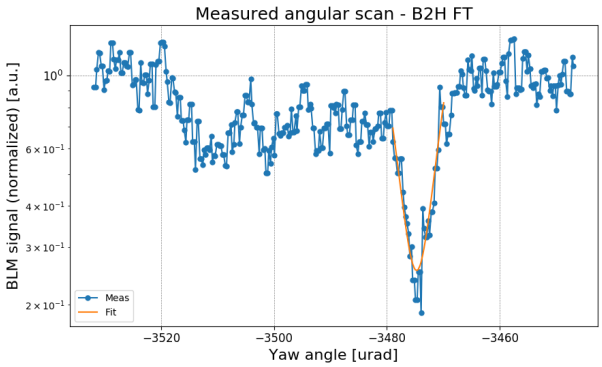

(c) B2H

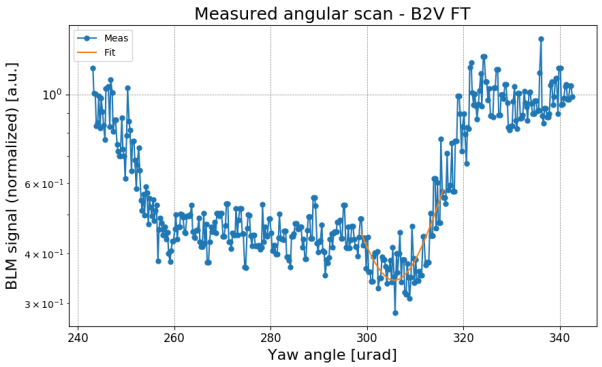

(d) B2V

Figure 3: Angular scans at flat top energy. The BLM signal has been normalized to the particle flux and to the amorphous level.

better understanding of the process. Since tracking simulations are not available for ions, these results could not be substantiated by comparing the angular scans with simulations.

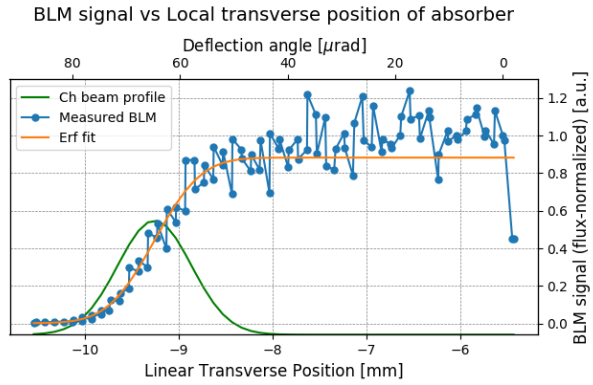

(a) B1H

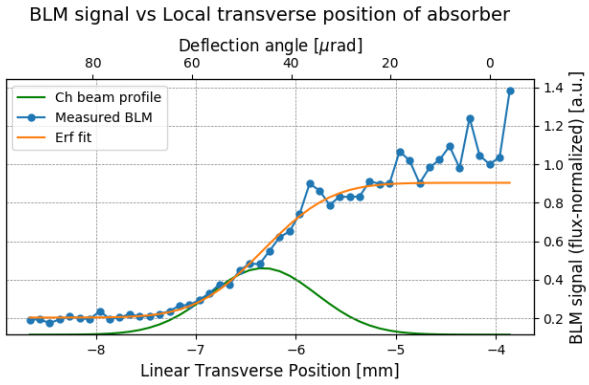

(b) B1V

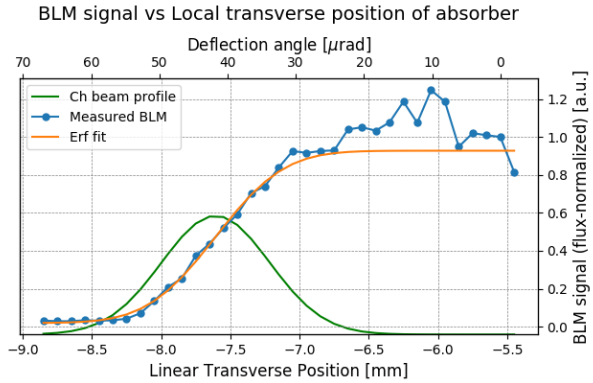

(c) B2H

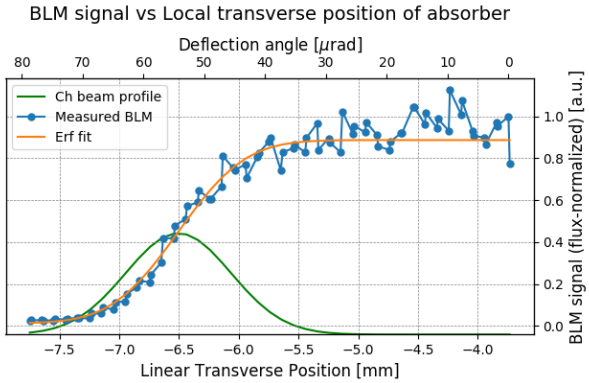

(d) B2V

Figure 4: Linear scans at injection energy. The BLM signal has been normalized to the particle flux and fitted with an error function to derive the bending angle of each crystal.

5 Loss Maps at Flat Top Energy

An extensive campaign of loss maps was carried out at flat top energy in order to compare the cleaning performances of the standard and crystal-assisted collimation system with different collimator settings. In particular (aside from the opening of the collimators upstream the crystals), two sets of configurations were tested:

1. TLCAs at progressively tighter settings: steps of one σ from 10 to 7 σ;
2. TCLAs and TCSGs downstream the crystals at progressively tighter settings: steps of one σ from 10 to 6 σ.

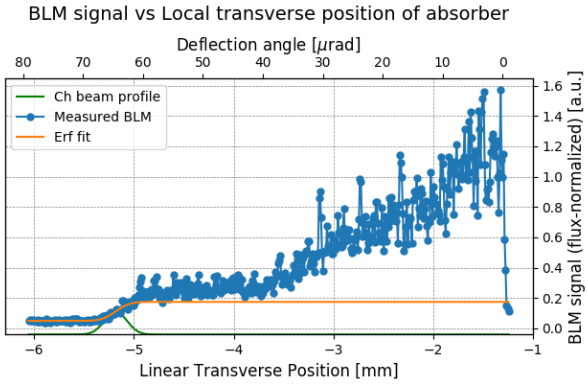

(a) B1H

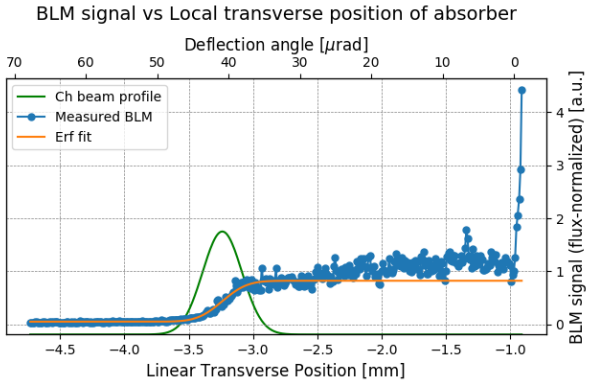

(b) B1V

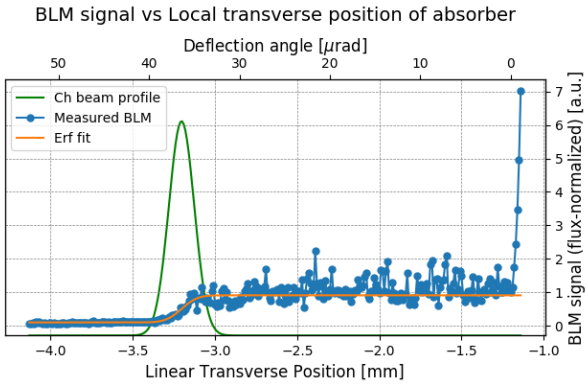

(c) B2H

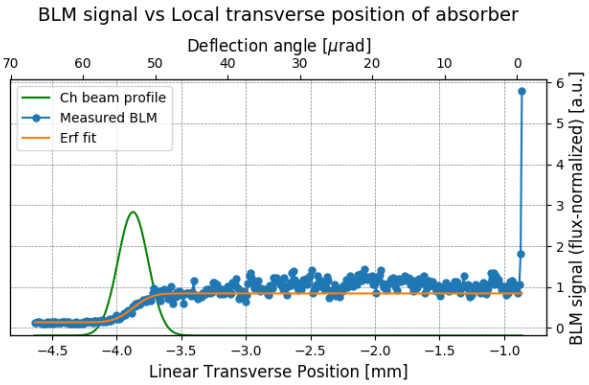

(d) B2V

Figure 5: Linear scans at flat top energy. The BLM signal has been normalized to the particle flux and fitted with an error function to derive the bending angle of each crystal.

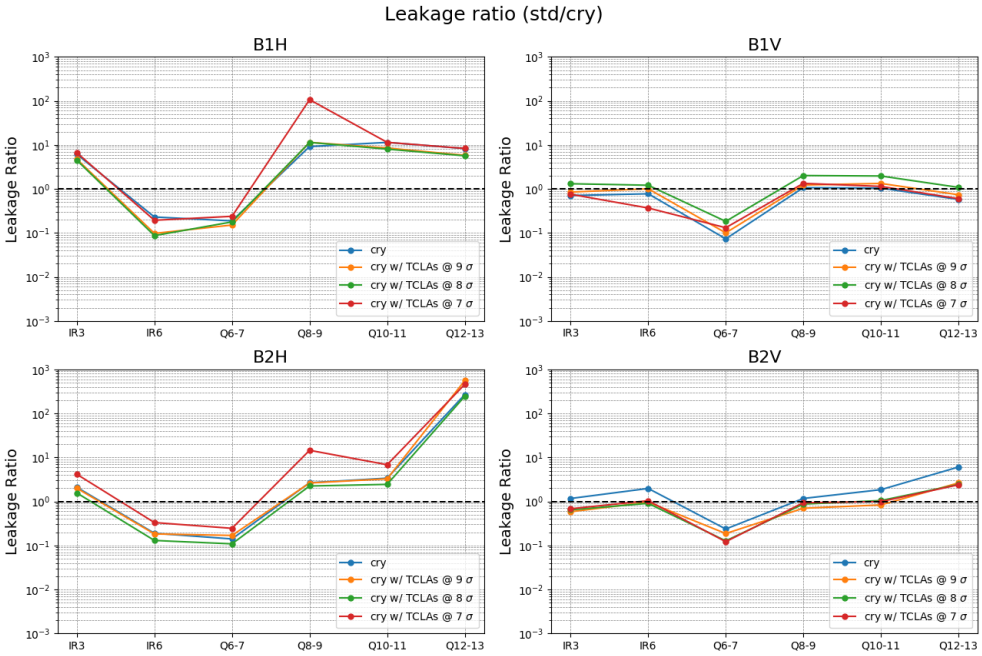

Figure 6: Ratio between losses measured with standard and crystal-assisted collimation system for each IR7 area. TCLAs have progressively tighter settings.

Each configuration is compared to the standard system with the same settings of TCSGs and TCLAs. The cold region in IR7 is divided into four areas identified by the quadrupoles they include, and the ratio between the losses measured with the standard and crystal-assisted collimation system is calculated for each of them. The highest losses on collimators in IR3 and IR6 are also measured.

The results are shown in Fig. 6 and 7. Different beams and planes show different behaviour. The horizontal crystals show the best results. In particular, B1H shows an improvement of a factor ∼10 when the crystal is deployed, and up to a factor ∼100 with optimized settings. B2H instead shows a factor ∼2-3 improvement, and up to a factor ∼10 with optimized settings. The vertical crystals on the other hand show lower gains. A possible explanation is the different production technologies, since the horizontal crystals are strip (ST) with the vertical ones are quasi-mosaic (QM). In QM crystals, the potential wells between crystalline planes do not have the same with and depth. This is not a problem for protons, but when the larger Pb ions are channeled by the smallest wells the probability of nuclear interaction increases. Losses in the Q7 region are higher with the crystal-assisted system in all cases. The current working hypothesis for the worse cleaning in Q7 attributes it to showers from upstream collimators. Simulation studies to confirm this hypothesis are currently on-going.

In all four planes, losses in IR3 are generally reduced when crystals are deployed, indicating reduced off-momentum debris emerging from IR7. On the other hand, losses in IR6 are higher because IR7-TCSGs with the same phase advance are retracted, causing an increased load.

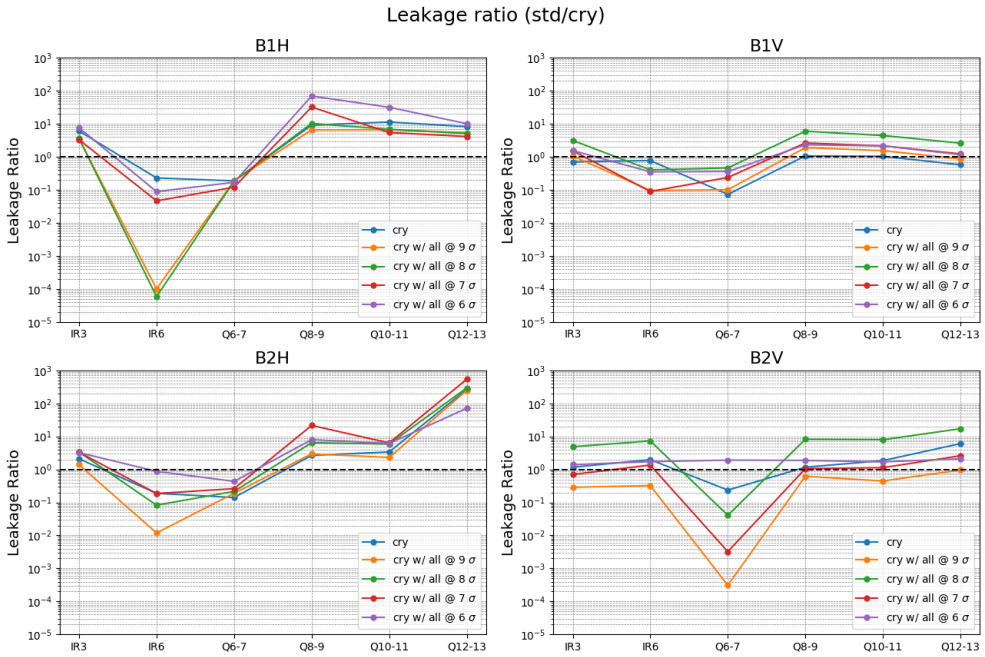

Figure 7: Ratio between losses measured with standard and crystal-assisted collimation system for each IR7 area. TCLAs and TCSGs downstream the crystals have progressively tighter settings.

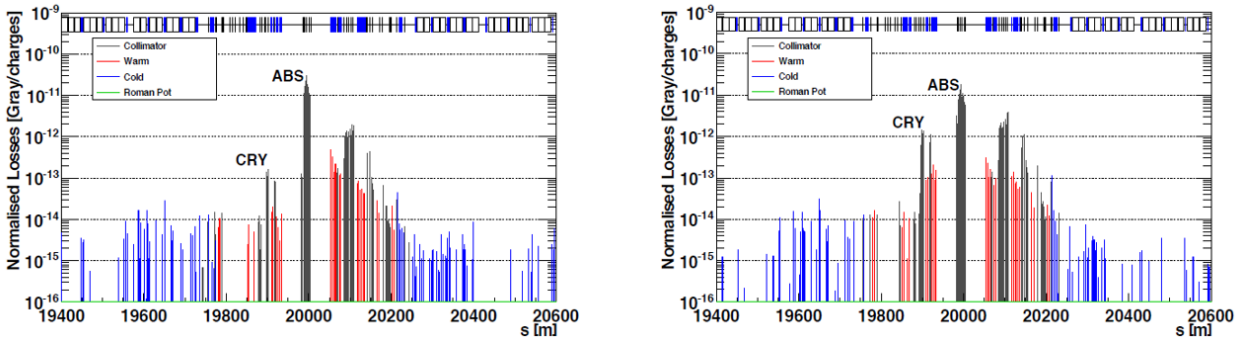

Figure 8: Loss pattern in IR7 during an angular scan when the crystal is oriented in channeling (left) and in amorphous (right). Losses are normalized to the beam flux. Crystal (CRY) and absorber (ABS) are shown on the plots [6, 9].

6 Crystal Channeling during Squeeze

Channeling conditions are assessed throughout dynamical phases of the machine, such as the squeeze, by means of continuous loss maps. When crystal-assisted collimation is in place and the crystal is in channeling orientation, losses at the crystal position are lower due to the reduction of nuclear interactions, while losses at the first collimator used as absorber increase. For this reason, the loss pattern in IR7 is different when the crystal is in channeling and amorphous conditions, as shown in Fig. 8. The ratio between losses at the crystal and the absorber can be used as a figure of merit. A ratio above 10^{-2} indicates that channeling conditions are lost [6, 9].

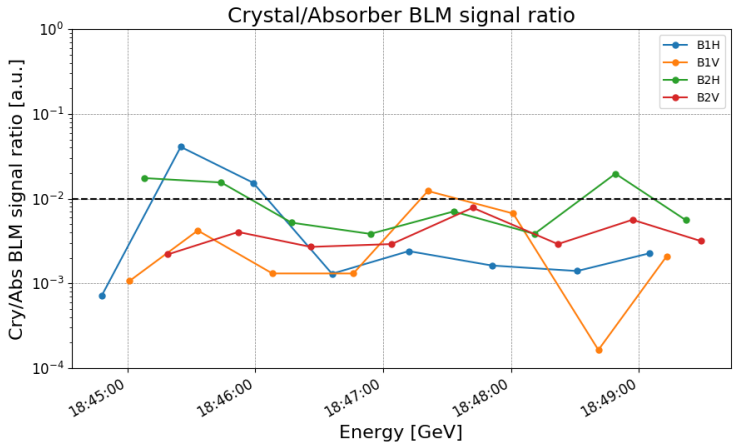

Figure 9: Ratio between losses at each crystal and at the corresponding absorber measured during the squeeze.

Loss maps were performed roughly every 30 seconds to evaluate the ratio throughout the squeeze. The results are shown in Fig. 9. The ratio stays under 10^{-2} for almost all points, indicating that channeling conditions were kept for all crystals during the whole squeeze.

7 Sustained Losses on Crystals

The MD ended with sustained losses on all four planes at the same time with crystals in channeling conditions for about 5 minutes. Fig. 10 shows the loss pattern while the blow up was active, along with the loss pattern observed during standard operation with ions. In both cases, the loss pattern in a moment in which the particle flux was roughly the same for the two beams is considered. The BLM signal is normalized to the respective flux of charges lost per second to allow a direct comparison. It is important to remember that the operational settings of the standard system have been optimized with long and hard work during commissioning [10, 11], in order to achieve the best cleaning performance. The crystal set up used in this MD is instead mainly focused on testing rather than actual operation, with many collimators (i.e. primaries and secondaries upstream the absorber of the channeled halo) open and in a non-optimized configuration.

Nevertheless, a qualitative comparison shows a generally cleaner loss pattern when crystals are deployed, with reduced losses in particular in IR6, IR3 and TCTs. This suggests that crystals are able to efficiently dispose of both fragments originated by the interaction of ions with the collimation system and off-momentum particles, whose production is reduced since the ions travel through the essentially empty space between crystalline place and the probability of nuclear interaction is reduced. Losses on cold magnets are also qualitatively reduced, with less loss spikes around the ring despite the ∼4 times larger loss rate achieved during the MD.

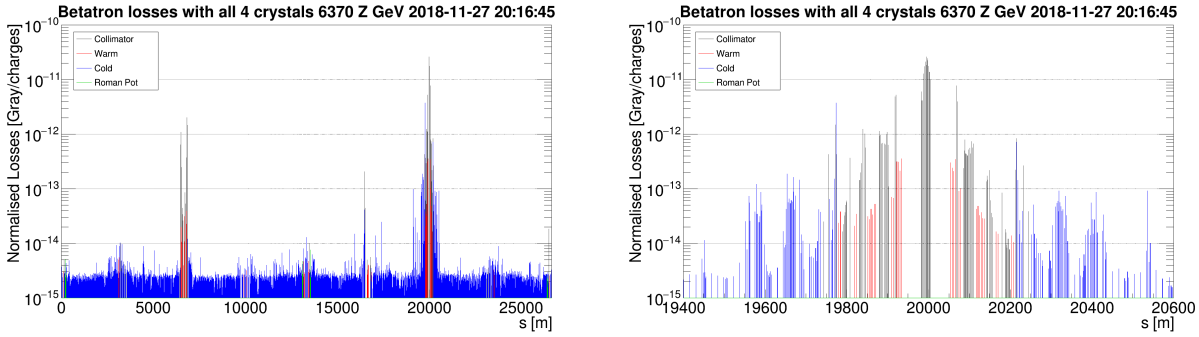

(a) Loss pattern with crystal collimation system, with active blow up on all beams and planes at the same time.

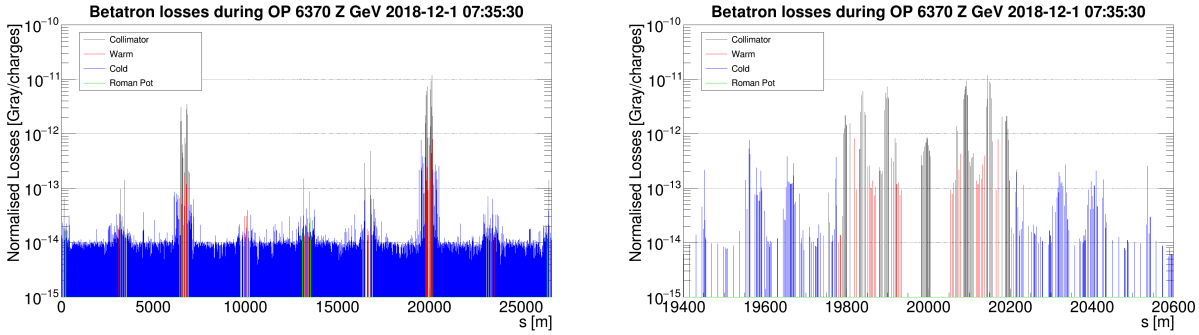

(b) Loss pattern during operation with ions, taken between the end of the energy ramp and the beginning of collisions.

Figure 10: Comparison of loss pattern with crystal and standard collimation system. The whole ring (left) and a zoom on IR7 (right) are shown. The BLM signal are normalized to the beam flux.

8 Acknowledgements

We would like to thank the OP crew for their assistance during the MD.

9 References

[1] D. Mirarchi, G. Hall, S. Redaelli, and W. Scandale, "Design and implementation of a crystal collimation test stand at the Large Hadron Collider," *The European Physical Journal C*, vol. 77, no. 6, p. 424, 2017.

[2] R. Rossi *et al.*, "Crystal collimation with protons at injection energy." CERN-ACC-NOTE-2016-0035.

[3] R. Rossi *et al.*, "Crystal collimation with protons at flat top energy." CERN-ACC-NOTE-2017-0021.

[4] R. Rossi *et al.*, "Crystal collimation cleaning measurements with proton beams in LHC." CERN-ACC-NOTE-2018-0024.

[5] R. Rossi *et al.*, "Beam 2 crystal characterization measurements with proton beams in the LHC." CERN-ACC-NOTE-2018-0067.

[6] R. Rossi, *Experimental assessment of crystal collimation at the Large Hadron Collider*. PhD thesis, Università degli Studi di Roma "La Sapienza", 2017.

[7] M. D'Andrea *et al.*, "Crystal collimation tests with proton beams." CERN-ACC-NOTE-2019-0022.

[8] M. D'Andrea *et al.*, "Operational aspects of crystal collimation with proton beams." CERN-ACC-NOTE-2019-0023.

[9] R. Rossi *et al.*, "Crystal collimation during the LHC energy ramp." CERN-ACC-NOTE-2018-0053.

[10] N. Fuster-Martínez *et al.*, "Summary and conclusions from loss map validation after TS2." 171st SPS and LHC Machine Protection Panel Meeting.

[11] N. Fuster-Martínez *et al.*, "2018 Heavy-ion loss maps validation." LHC Collimation Working Group #236.